

# High-Strength Al-Based Bulk Alloy Produced by Spark Plasma Sintering of Gas Atomized Powders

*Nguyen Hoang Viet*

*Hanoi University of Science and Technology – No. 1, Dai Co Viet Str., Hai Ba Trung, Ha Noi, Viet Nam*

*Received: November 09, 2018; Accepted: June 24, 2019*

## Abstract

*In this work, consolidation of gas atomized  $Al_{84}Gd_6Ni_7Co_3$  glassy powders into highly dense bulk specimens was carried out by spark plasma sintering. The highest relative density and hardness value can be obtained for sample sintered at 613 K are about 99.7 % and 495 HV, respectively. Room temperature compression tests of the consolidated bulk material reveal remarkable mechanical properties, namely, high compression strength of 1020 MPa with maximum elongation of 3.2 %, but without plastic deformation. The failure morphology of the sintered sample surface presented a transparticle fracture mechanism, indicating the efficiency of the sintering processing.*

Keywords: bulk amorphous alloys, spark plasma sintering, Al-based alloys

## 1. Introduction

Amorphous Al-based alloys ( $\geq 80\%$  at.% Al) containing rare earth and transition metal solutes possess high ultimate strength, ductility and corrosion resistance [1-3], as compared with the conventional alloys. Such high strength materials are particularly attractive for automobile and aerospace [4, 5]. The mechanical properties can be further improved by the partial crystallization of Al-based amorphous precursors to create a homogeneous distribution of nanoscale fcc-Al or nanosized intermetallic compounds within a residual amorphous matrix [6, 7]. Normally, Al-based metallic glasses have been synthesized successfully by rapid quenching, such as melt-spinning technique [8]. However, Al-based metallic alloys are generally produced in form of thin ribbons [9]. Therefore, attempts have been made to produce Al-based metallic alloy powder using gas atomization receiving much attention to materials scientists. This technique is the most potential technique for commercialization due to high cooling rate during solidification and mass productivity [10]. Among the different consolidation techniques, spark plasma sintering (SPS) has been recognized as a suitable technique to obtain highly dense samples with desired microstructure and properties. SPS offer many advantages over conventional sintering methods such as hot press sintering, hot isostatic pressing or atmospheric furnaces, including ease of operation, high sintering speed, high reproducibility, safety and reliability. With high heating rate and short

holding time, bulk samples after sintering can be retained amorphous structure [11, 12].

In this work, amorphous  $Al_{84}Gd_6Ni_7Co_3$  gas-atomized powders were consolidated by SPS. Phase analysis of glassy powders and sintered samples were determined using XRD method. Densification tests and mechanical behavior of compacted samples were evaluated by micro-hardness and compression tests followed by failure analysis.

## 2. Experimental

Powders with nominal composition  $Al_{84}Gd_6Ni_7Co_3$  (purity  $> 99.9$  wt.%) were prepared by gas atomization. Particle size distribution of the sample was measured using a Malvern Panalytical's Mastersizer 2000 laser diffractometer. The powders were consolidated into cylindrical specimens of 10 mm diameter under high vacuum using the SPS-515 Sumitomo Coal Mining spark plasma sintering equipment. The chamber was evacuated to a pressure  $< 5$  Pa. The mold and punches are made of the WC-Co alloy. An amount of 1.5 g of amorphous powders were spark plasma sintered at 543, 578 and 613 K, at a heating rate of 10 K/min and applied pressures of 500 MPa during 3 min of holding time. Relative densities of bulk samples were evaluated by Olympus PMG3 optical microscope (Olympus Corporation, Tokyo, Japan) with computerized image analysis at a magnification of  $100\times$ . The microstructure was characterized by XRD in a SIEMENS D5000 diffractometer using Cu-K $\alpha$  radiation and FE-SEM using a JEOL JSM 6500 F microscope. Compression tests of sintered samples were done with an INSTRON 4469 testing facility with a normal displacement rate of  $1.67\times 10^{-3}$  s $^{-1}$  at room

\* Corresponding author: Tel.: (+84) 904.777.570  
Email: viet.nguyenhoang@hust.edu.vn

temperature. Vickers microhardness measurements were performed using a Mitutoyo MVK-H1 Hardness Testing Machine under a load of 50 g.

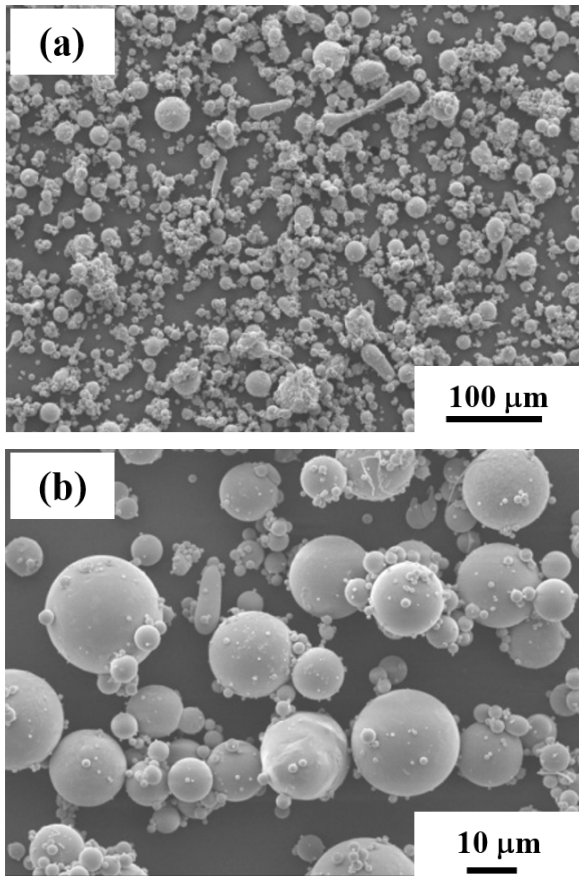


**Fig. 1.** FE-SEM images of  $\text{Al}_{84}\text{Gd}_6\text{Ni}_7\text{Co}_3$  GA powders at different magnification (a) X200 and (b) X1000.

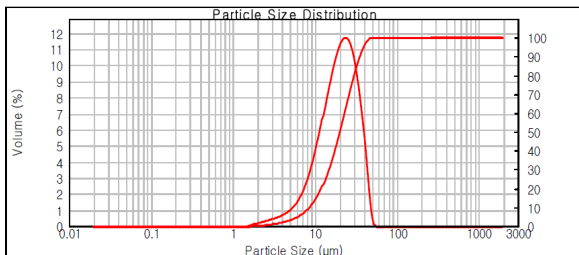


**Fig. 2.** Particle size distributions of amorphous  $\text{Al}_{84}\text{Gd}_6\text{Ni}_7\text{Co}_3$  GA powders.

### 3. Results and discussion

Fig.1 (a) shows the SEM images gas atomized (GA)  $\text{Al}_{84}\text{Gd}_6\text{Ni}_7\text{Co}_3$  powders. Almost all of powders have spherical shape and smooth surface. Small particle powders (diameter  $< 1 \mu\text{m}$ ) are around the bigger particles (diameter is about  $20 \mu\text{m}$ ) as seen in Fig.1 (b). Particle size distribution of the GA powders was measured by means of laser light-scattering granulometry as shown on Fig.2. The sample has a

unimodal distribution and an average particle size,  $d_{0.5}$ , of about  $19.86 \mu\text{m}$ .

Fig.3 (a-b) shows the curves of change in Z-displacement and Z-displacement rate of GA  $\text{Al}_{84}\text{Gd}_6\text{Ni}_7\text{Co}_3$  powders during the sintering process at temperature 723 K, 3 min holding time, under pressures of 500 MPa, respectively. There is a maximum Z-displacement rate around 486 K. The thermally activated expansion stage can be seen from 300 to 420 K. Then shrinkage can be observed starting at 420 until the maximum shrinkage rate at 486 K. Shrinkage rate decline from 486 to 543 K and fall continuously to 648 K. There is a small change in shrinkage rate near 648 K. At holding stage, the shrinkage is increased slightly.

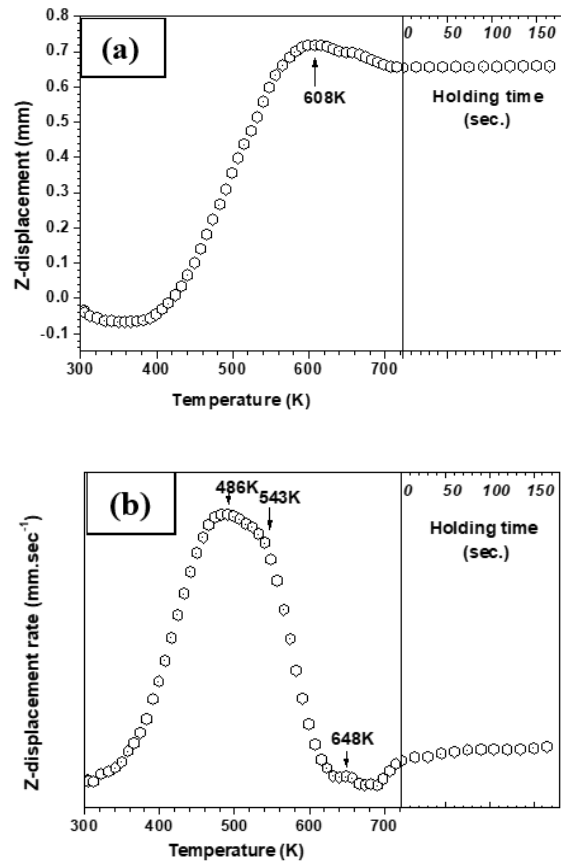


**Fig. 3.** Sintering curves of GA powders - change in (a) Z-displacement and (b) Z-displacement rate sintered at 723 K.

Fig.4 shows XRD patterns of GA powders and samples sintered at different temperatures. All XRD patterns at sintering temperature below 543 K shows a halo peak (characteristic of the amorphous phase) and the peaks of fcc-Al (Fig.4 (a-c)). At highest sintering temperature of 613 K, besides diffraction peaks of fcc-Al nano-crystalline, an intermetallic phase of  $\text{Al}_{19}\text{Gd}_3\text{Ni}_5$  can be detected (Fig.4d). This intermetallic phase is detected from similar sample

which was heated in the differential scanning calorimetry [13].

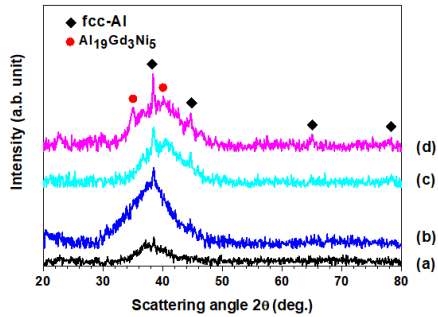


**Fig. 4.** XRD patterns of samples (a) GA powders, SPS at (b) 543, (c) 578, and (d) 613K.

The optical microscopic images of polished surface of bulk samples are shown in Fig.5 (a-c). Pores (dark-gray contrast) occur clearly throughout the sample sintered at 543 K. The pores were rapidly removed at higher sintering temperatures of 578 K. The highest relative density of 99.7 % can be obtained for sample sintered at 613 K.

The hardness of sintered samples increases from 312 to 495 HV with increasing sintering temperature from 543 to 613 K, respectively as seen in table 1. The room temperature compression test (strain rate of  $1.67 \times 10^{-3} \text{ s}^{-1}$ ) of  $\text{Al}_{84}\text{Gd}_6\text{Ni}_7\text{Co}_3$  sample sintered at 613 K is presented in Fig.6. The crystallization during consolidation occurs leading to bulk sample with a remarkably high-strength of about 1020 MPa and elongation of 3.2 %. This high-strength is due to a possible preparation of a composite alloy of fcc-Al nanoparticles + amorphous phase which has quite remarkable mechanical properties (about three times larger than the conventional high-strength Al-based alloys) [14, 15]. Zhi Wang et al. [7] reported that the confining effect could effectively suppress the premature brittle fracture of the intermetallics and the nanocrystalline fcc-Al to achieve such a high strength.

Post-compression SEM images of a compressive tested specimen of solid-state sintered at 613 K show morphology of fractured surface in Fig.7. A viewing of fractography of fractured  $\text{Al}_{84}\text{Gd}_6\text{Ni}_7\text{Co}_3$  compact surface indicates that the sample was dense. The crack was partly formed by transparticle fracture and developed along the interparticle of the powder which is similar as observing for fracture surface of SPSed  $\text{Al}_{82}\text{La}_{10}\text{Fe}_4\text{Ni}_4$  sample [16].

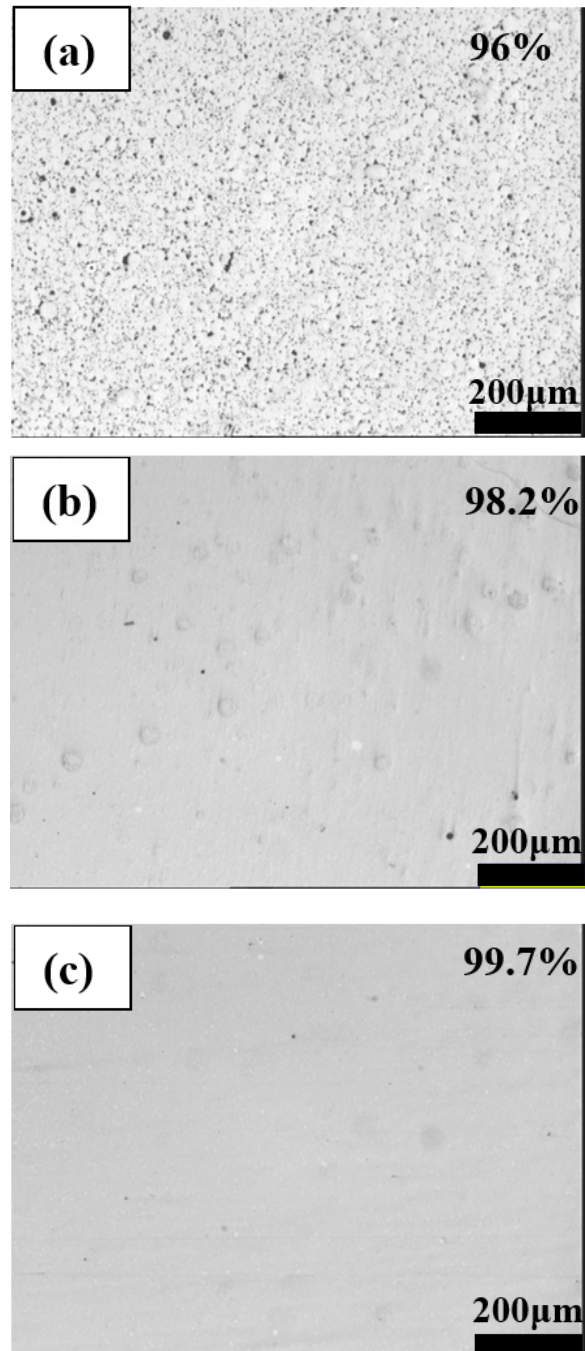


**Fig. 5.** Optical micrographs of polished surface of samples after sintered at (a) 543, (b) 578 and (c) 613K.

**Table 1.** Hardness values of  $\text{Al}_{84}\text{Gd}_6\text{Ni}_7\text{Co}_3$  sintered samples

Sintering temperature (K)	543	578	613
Hardness (HV)	312	445	495

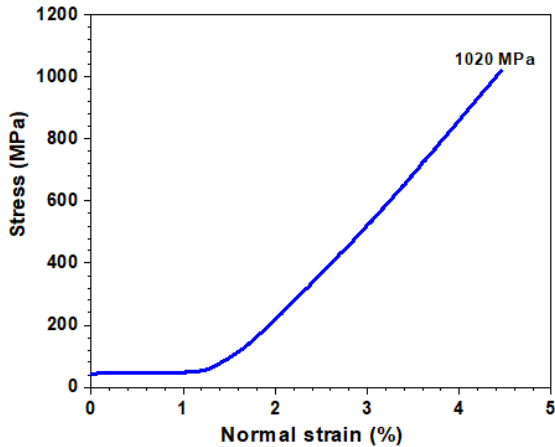


Fig. 6. Compression test of Al<sub>84</sub>Gd<sub>6</sub>Ni<sub>7</sub>Co<sub>3</sub> sample sintered at 613 K.

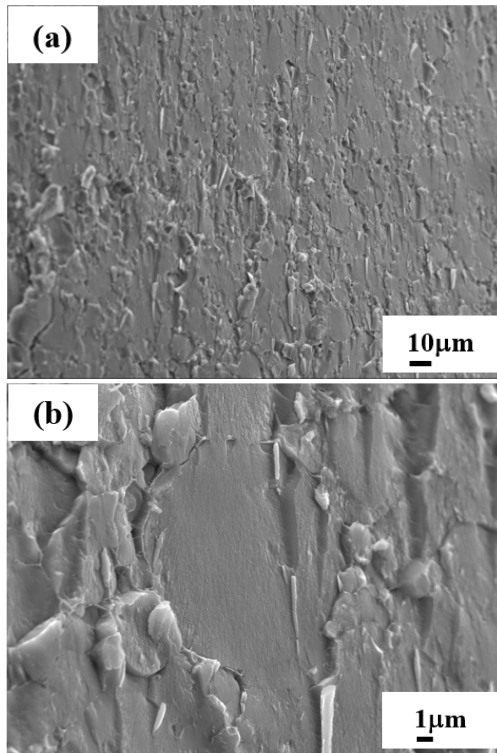


Fig. 7. Fracture surface of post-compressive test of sample sintered at 613K at different magnifications (a) X 500 and (b) X 10000.

#### 4. Conclusion

The bulk high-strength Al<sub>84</sub>Gd<sub>6</sub>Ni<sub>7</sub>Co<sub>3</sub> alloy samples were produced by SPS at different sintering temperatures. The sintering behavior of the amorphous Al<sub>84</sub>Gd<sub>6</sub>Ni<sub>7</sub>Co<sub>3</sub> alloy shows a maximum in shrinkage rate around 486 K. Samples sintered at 613 K partly crystallization with fcc-Al and an intermetallic compound of Al<sub>19</sub>Gd<sub>3</sub>Ni<sub>5</sub>. The relative density is increased from 96 to 99.7 % with

increasing sintering temperatures from 543 to 613 K, respectively. The highest hardness value is about 495 HV for sample sintered at 613 K. The consolidated bulk material exhibits a high compressive strength of 1020 MPa with maximum elongation of 3.2% without plastic deformation. Porosity was ascertained as being the responsible for this behavior. The morphology of the failure surface of the bulk Al<sub>84</sub>Gd<sub>6</sub>Ni<sub>7</sub>Co<sub>3</sub> alloy shows the transparticle-fracture mechanism, indicating the efficiency of the sintering condition.

#### Acknowledgments

The author would like to thank Prof. Ji-Soon Kim and Prof. Jürgen Eckert for raw materials and SPS facility.

#### References

- [1]. S. Scudino, K.B. Surreddi, S. Sager, M. Sakaliyska, J.S. Kim, W. Löser, J. Eckert; Production and mechanical properties of metallic glass-reinforced Al-based metal matrix composites; *Journal of Materials Science* 43(13) (2008) 4518–4526.
- [2]. H. Nitsche, F. Sommer, E.J. Mittemeijer; The Al nano-crystallization process in amorphous Al<sub>85</sub>Ni<sub>8</sub>Y<sub>5</sub>Co<sub>2</sub>; *Journal of Non-Crystalline Solids* 351(49) (2005) 3760-3771.
- [3]. A. Inoue, Y. Horio, T. Masumoto; New Amorphous Al-Ni-Fe and Al-Ni-Co Alloys; *Materials Transactions, JIM* 34(1) (1993) 85-88.
- [4]. L.-C. Zhuo, S.-J. Pang, H. Wang, T. Zhang; Ductile Bulk Aluminum-Based Alloy with Good Glass-Forming Ability and High Strength; *Chinese Physics Letters* 26(6) (2009) 066402.
- [5]. T.T. Sasaki, K. Hono, J. Vierke, M. Wollgarten, J. Banhart; Bulk nanocrystalline Al<sub>85</sub>Ni<sub>10</sub>La<sub>5</sub> alloy fabricated by spark plasma sintering of atomized amorphous powders; *Materials Science and Engineering: A* 490(1) (2008) 343-350.
- [6]. J. Basu, S. Ranganathan; Crystallisation in Al-ETM-LTM-La metallic glasses; *Intermetallics* 12(10) (2004) 1045-1050.
- [7]. Z. Wang, R.T. Qu, S. Scudino, B.A. Sun, K.G. Prashanth, D.V. Louzguine-Luzgin, M.W. Chen, Z.F. Zhang, J. Eckert; Hybrid nanostructured aluminum alloy with super-high strength; *Npg Asia Materials* 7 (2015) e229.
- [8]. C. Suryanarayana, A. Inoue; *Bulk Metallic Glasses*; 2nd Edition ed., CRC Press, 2011.
- [9]. Á. Révész, L.K. Varga, S. Suriñach, M.D. Baró; Thermal stability, crystallization kinetics, and grain growth in an amorphous Al<sub>85</sub>Ce<sub>5</sub>Ni<sub>8</sub>Co<sub>2</sub> alloy; *Journal of Materials Research* 17(8) (2011) 2140-2146.
- [10]. J.C. Kim, H.J. Ryu, J.S. Kim, B.K. Kim, Y.J. Kim, H.J. Kim; Synthesis and densification of Cu added Fe-based BMG composite powders by gas

- atomization and electrical explosion of wire; Journal of Alloys and Compounds 483(1) (2009) 28-31.
- [11]. T. Gheiratmand, H.R. Madaah Hosseini, P. Davami, C. Sarafidis; Fabrication of FINEMET bulk alloy from amorphous powders by spark plasma sintering; Powder Technology 289 (2016) 163-168.
- [12]. S.P. Harimkar, T. Borkar, A. Singh; Spark plasma sintering of amorphous-crystalline laminated composites; Materials Science and Engineering: A 528(3) (2011) 1901-1905.
- [13]. Z. Wang, K.G. Prashanth, S. Scudino, J. He, W.W. Zhang, Y.Y. Li, M. Stoica, G. Vaughan, D.J. Sordelet, J. Eckert; Effect of ball milling on structure and thermal stability of  $\text{Al}_{84}\text{Gd}_6\text{Ni}_7\text{Co}_3$  glassy powders; Intermetallics 46 (2014) 97-102.
- [14]. J. Eckert, M. Calin, P. Yu, L.C. Zhang, S. Scudino, C. Duhamel; Al-Based Alloys Containing Amorphous and Nanostructured Phases; Reviews on advanced materials science 18 (2018) 169-172.
- [15]. Y.-H. Kim, A. Inoue, T. Masumoto; Increase in Mechanical Strength of Al-Y-Ni Amorphous Alloys by Dispersion of Nanoscale fcc-Al Particles; Materials Transactions, JIM 32(4) (1991) 331-338.
- [16]. H.N. Viet, T.N. Oanh, J.-S. Kim, M.A. Jorge; Crystallization Kinetics and Consolidation of  $\text{Al}_{82}\text{La}_{10}\text{Fe}_4\text{Ni}_4$  Glassy Alloy Powder by Spark Plasma Sintering; Metals 8(10) (2018), 812.